Nonparallel spatial stability of the boundary layer induced by Long's vortex on a solid plane perpendicular to its axis

L. Parras and R. Fernandez-Feria
E.T.S. Ingenieros Industriales, Universidad de Málaga (Spain)
(Received 28 July 2004; revised manuscript received 26 January 2005; published 21 September 2005)

We consider the linear, viscous stability of the boundary layer induced by an unbounded vortex whose outer inviscid structure coincides near the axis with Long's vortex. The viscous boundary layer induced by the interaction of such a vortex with a solid plane perpendicular to the axis has a known self-similar structure. The spatial stability of this self-similar solution is analyzed here for axisymmetric and nonaxisymmetric perturbations propagating towards the axis of rotation. Viscous and nonparallel effects on the stability of the perturbations are retained up to their first order in the inverse of the local Reynolds number (nondimensional radius). The resulting parabolic stability equations are solved numerically using a spectral collocation method varying both the nondimensional frequency and radius. It is found that the flow is unstable to axisymmetric perturbations far away from the axis (inviscid instability). The growth rate of this inertial instability mode first increases and then decreases as the Reynolds number decreases (as the axis is approached). However, before this inviscid mode becomes stabilized, new viscous instabilities for both axisymmetric and nonaxisymmetric perturbations show up, which finally become stabilized at moderate Reynolds numbers. We characterize the critical Reynolds numbers and frequencies for the stability of these unstable perturbations as functions of their azimuthal wave number. It is found that the last perturbations that become stable as the axis is approached are nonaxisymmetric, corotating, perturbations with an azimuthal wave number $n=4$.

DOI: 10.1103/PhysRevE.72.036305 PACS number(s): 47.20.−k, 47.15.Cb, 47.32.Cc

I. INTRODUCTION

The viscous interaction of a free vortex with a solid surface perpendicular to the vortex axis is a problem of engineering and geophysical (atmospheric) interest. Very little is known about the structure and stability of such an interaction for physically relevant vortices. In this work we consider the linear, viscous stability of the boundary layer induced by an unbounded vortex whose outer inviscid structure coincides near the axis with Long's vortex [1], a well-known flow that has been commonly used to model intense atmospheric vortices such as tornadoes [2–4]. The viscous boundary layer induced by the interaction of these vortices with a solid plane perpendicular to its axis was considered in Ref. [5], where a self-similar structure (of the second kind) was found. As the axis of symmetry is approached, this self-similar solution takes a relatively simple form, which is obviously not valid very near the axis, where the flow turns upward to form the rising viscous core of the vortex [6]. The structure of this effusing core flow cannot be modeled by a boundary-layer approximation. One has to solve the full [three-dimensional (3D)] incompressible Navier-Stokes equations numerically to close the problem. But before undertaking such a numerical approach, it is of interest to have some knowledge of the stability of this boundary layer flow, which constitutes the boundary condition for radially incoming flow in the numerical approach. In particular, one would like to know the range of Reynolds numbers for which the self-similar boundary layer flow is stable to nonaxisymmetric perturbations.

The spatial stability of the self-similar solution to the boundary layer equations given in Ref. [5] is analyzed here for both axisymmetric and nonaxisymmetric perturbations propagating towards the axis of rotation. The first task will be to characterize this incoming flow with the minimum number of dimensionless parameters. This is made in the next section, together with a brief discussion of the physical relevance of these vortices. Then, the spatial stability problem is formulated in Sec. III. Viscous and nonparallel effects on the stability of the perturbations are retained up to the order of the inverse of the local Reynolds number which, as we shall see, is equivalent to a nondimensional radius in the formulation given in this work. The results of the stability analysis are described in Sec. IV, and some conclusions are drawn in the last section.

II. BOUNDARY LAYER VORTEX

A. Structure of the basic flow

Experimental measurements in a wide class of both confined and open intense vortices (vortex chambers, tornadoes, etc.; see, e.g., Ref. [7]) show that their azimuthal velocity decays as a power of the distance r to the axis of rotation ranging between -0.4 and -1 and that they all have an important meridional velocity field superimposed onto the circumferential motion. These characteristics are both met by the family of self-similar solutions for high Reynolds numbers to the Navier-Stokes equations given in Refs. [4,8]. In cylindrical polar coordinates (r,θ,z), the structure of the inviscid, outer velocity field has the form

$$\mathbf{v} \equiv (u,v,w) = \mathbf{V}(y) r^{m-2}, \quad y \equiv \frac{r}{z}, \tag{1}$$

where $0 \leqslant m \leqslant 2$ and the vector function $\mathbf{V}(y)$ is characterized by the swirl parameter L, or ratio of near-axis inviscid azimuthal velocity to axial velocity,

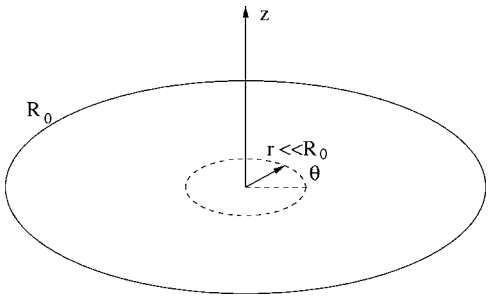

FIG. 1. Sketch of the coordinate system.

$$L = (v/w)_{y=0}. \tag{2}$$

For simplicity sake and as representative case of this family of vortices, we shall consider here only the case $m=1$, which near the axis constitutes the outer inviscid velocity field of the well known Long's vortex [1,4], though the formulation will be given for any value of m.

It was shown in Ref. [5] that the viscous boundary layer induced by an inviscid vortex such as Eq. (1) on a solid infinite plane perpendicular to the axis ($z=0$) has no self-similar structure. In other words, no self-similar solution of the first kind exists connecting the no-slip boundary condition at the plane with the inviscid outer vortex, a peculiar feature shared by other inviscid vortices *without* meridional motion [9,10]. However, it was found that a self-similar solution of the second kind does exist. This solution, which was corroborated by solving numerically the boundary layer equations, has the formal difficulty that is defined in terms of an additional scale length R_0, which represents the radius of the arbitrary solid disk perpendicular to the axis on which the finite viscous boundary layer is developed (see Fig. 1 for a sketch of the flow geometry). Nonetheless, near the axis, when $r \ll R_0$, this self-similar structure of the second kind for the boundary layer structure can be written in a simple form which will allow us to solve the stability problem without taking into account the scale length R_0 explicitly.

In fact, with errors of the order of $(r/R_0)^3 \ll 1$, the velocity (u,v,w) and pressure (p) fields in the boundary layer can be written as [5]

$$u = -u_0 f'(\eta), \tag{3}$$

$$v = \frac{u_0}{\sqrt{R}} g(\eta), \tag{4}$$

$$w = \frac{u_0}{R} \eta f'(\eta), \tag{5}$$

$$p/\rho = u_0^2 R^{m+2}\, \mathrm{Re}^{-8/(m+2)}\, \Pi_0, \tag{6}$$

where the nondimensional axial and radial coordinates inside the boundary layer are

$$\eta \equiv \frac{z}{\delta(r)}, \quad R \equiv \frac{r}{\delta(r)}, \tag{7}$$

and the boundary layer thickness is given by

$$\delta(r) = \frac{R_0^2\, \mathrm{Re}^{-2/(m+2)}}{r}. \tag{8}$$

In these expressions,

$$\mathrm{Re} \equiv (KQ)^m R_0^{m-1}/\nu \gg 1 \tag{9}$$

is a Reynolds number for the external vortex based on the length scale R_0, where K is related to its circulation and Q to the swirl parameter L, Eq. (2), through [4,8]

$$D = \frac{2-m-(m-1)L^2}{m^3 L^4}, \quad Q = \left(\frac{4D}{m(2-m)}\right)^{1/4}. \tag{10}$$

The characteristic velocity u_0 appearing in Eqs. (3)–(6) is given by

$$u_0 = \frac{\nu}{R_0}\, \mathrm{Re}^{4/(m+2)}, \tag{11}$$

while Π_0 is a constant that depends on m and L (its value is not relevant here because the pressure of the basic flow does not enter into the linear stability analysis). Finally, the functions $f(\eta)$ and $g(\eta)$ are governed by the following equations and boundary conditions:

$$f''' + \frac{3m}{m+2} f f'' + \frac{3(2-m)}{m+2} f'^2 = 0, \tag{12}$$

$$g'' + \frac{3(1-m)}{m+2} g f' + \frac{3m}{m+2} f g = 0, \tag{13}$$

$$\eta = 0, \quad f = f' = g = 0, \tag{14}$$

$$\eta \to \infty, \quad f \to \eta^{m/2}, \quad g \to Q^{-1} \eta^{(m-1)/2}, \tag{15}$$

where the primes denote derivatives with respect to η. That the velocity field is given by just two functions f and g is related to the fact that the meridional flow is fully characterized by a stream function Ψ ($ru = -\partial\Psi/\partial z$, $rw = \partial\Psi/\partial r$), which is proportional to $f(\eta)$.

As already mentioned, we shall consider in what follows only the case $m=1$ (Long's vortex) with $L=\sqrt{2}$, which is the unique value of the swirl parameter allowed for $m=1$ by the viscous regularity of the inviscid vortex at the axis [1,4]. For this case, $D=1/4$ and $Q=1$ in Eqs. (10). Figure 2 depicts the functions $f(\eta)$, $g(\eta)$, and some of their derivatives for this case.

B. Reynolds number and nondimensional radius

The above boundary layer approximation is valid for $\mathrm{Re} \gg 1$ when $r \ll R_0$ [terms of the order of $(r/R_0)^3$ and $O(\mathrm{Re}^{-2/(m+2)})$ have been neglected [5]]. In addition, r must be large compared to the boundary layer thickness $\delta(r)$—i.e., $R \gg 1$. From Eqs. (7) and (8), the relation between the nondimensional radius R and the Reynolds number Re is

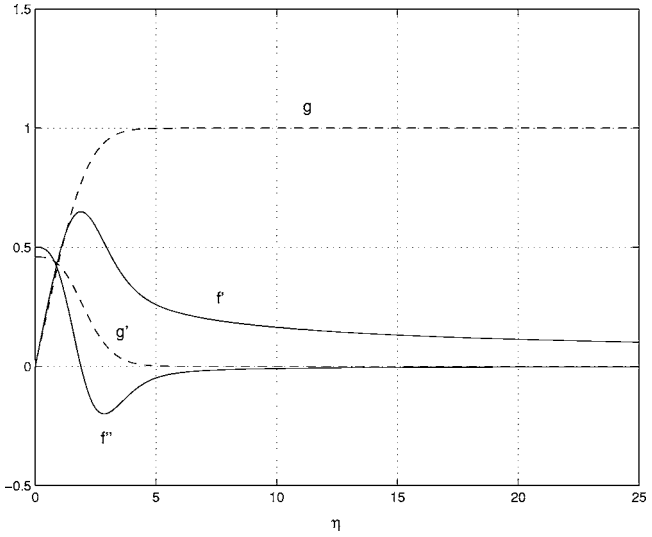

FIG. 2. Self-similar boundary layer solution.

$$R = \left(\frac{r}{R_0}\right)^2 \mathrm{Re}^{2/(m+2)}. \tag{16}$$

The above inequalities tell us that the stability analysis given in this work will be valid in the following range of values of r:

$$\mathrm{Re}^{-1/(m+2)} \ll \frac{r}{R_0} \ll 1 \tag{17}$$

or

$$1 \ll R \ll \mathrm{Re}^{2/(m+2)}. \tag{18}$$

Since the scale length R_0 is chosen arbitrarily, these conditions can always be met with sufficient amplitude provided that $\mathrm{Re} \gg 1$. It might also be noted that, owing to the condition $R \gg 1$, $u \gg v \gg w$ in the basic flow [see Eqs. (3)–(5)].

In terms of R and Re, the scale length R_0 will not appear explicitly in the nondimensional stability problem. Given r/R_0 (and m) Eq. (16) provides the relation between R and Re. This relation is plotted in Fig. 3 for $m=1$ and $(r/R_0)^3 = 0.1$, which are the numerical values used in this work. As the controlling parameter we shall use R. We start from $R \to \infty$ (inviscid stability) and decrease it until R becomes of order unity, where the analysis is no longer valid. To account for both the nonparallel effects and the viscous terms consistently in the stability equations, we will retain terms up to $O(R^{-3/2})$ and $O(R^{1/2}\,\mathrm{Re}^{-3/(m+2)})$ (see next section). The results in terms of R (or Re) are universal and independent of R_0. What will change with R_0 is the relation between Re and R.

III. STABILITY FORMULATION AND NUMERICAL METHOD

To analyze the linear stability of the above basic flow, the flow variables (u, v, w) and p, are decomposed, as usual, into their mean parts, Eqs. (3)–(6), and small perturbations,

$$u = u_0(-f' + \bar{u}), \tag{19}$$

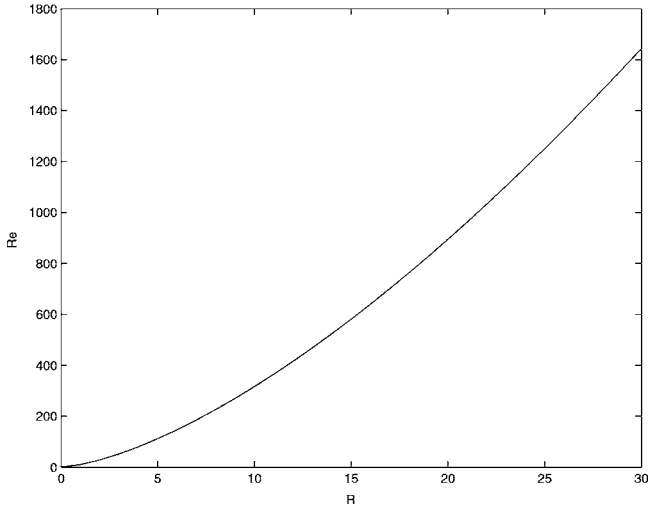

FIG. 3. Re vs R for $m=1$ and $(r/R_0)^3=0.1$.

$$v = u_0\left(\frac{g}{\sqrt{R}} + \bar{v}\right), \tag{20}$$

$$w = u_0\left(\frac{\eta f'}{R} + \bar{w}\right), \tag{21}$$

$$p/\rho = u_0^2\left(R^{m+2}\,\mathrm{Re}_{CL}^{-8/(m+2)}\Pi_0 + \bar{p}\right). \tag{22}$$

The nondimensional perturbations $\mathbf{s} \equiv [\bar{u}, \bar{v}, \bar{w}, \bar{p}]^T$ are decomposed in the standard form:

$$\mathbf{s}(R, \eta, \theta, t) = \mathbf{S}(R, \eta)\chi(R, \theta, t), \tag{23}$$

where the complex amplitude

$$\mathbf{S}(R, \eta) \equiv \begin{pmatrix} F(R, \eta) \\ G(R, \eta) \\ H(R, \eta) \\ \Pi(R, \eta) \end{pmatrix} \tag{24}$$

depends on both the radial and axial coordinates. The other part of the perturbation is of exponential form and describes the wavelike nature of the disturbance,

$$\chi(R, \theta, t) = \exp\left[\int_{R_i}^{R} a(R')dR' + i(n\theta - \omega t)\right], \tag{25}$$

where R_i is an initial or reference radius (or Reynolds number). The nondimensional, order of unity, complex radial wave number a is defined as

$$a(R) \equiv \gamma(R) + i\alpha(R). \tag{26}$$

The real part $\gamma(R)$ is the local exponential growth rate, and the imaginary part $\alpha(R)$ is the local radial wave number. A nondimensional frequency ω has also been defined. Finally, the azimuthal wave number n is equal to zero for axisymmetric perturbations and different from zero for spiral perturbations.

Substituting Eqs. (23)–(25) into the incompressible Navier-Stokes equations and neglecting both second-order

terms in the small perturbations and terms $O(R^{-2})$, retaining only the lowest-order viscous terms, the following set of linear parabolic stability equations (PSEs) results:

$$\mathbf{L}\cdot\mathbf{S}+\mathbf{M}\cdot\frac{\partial\mathbf{S}}{\partial R}=0, \tag{27}$$

$$\mathbf{L}=\mathbf{L}_1+a\mathbf{L}_2+\frac{1}{\sqrt{R}}\mathbf{L}_3+\frac{1}{R}\mathbf{L}_4+\frac{1}{R^{3/2}}\mathbf{L}_5 - \frac{\sqrt{R}}{\mathrm{Re}^{3/(m+2)}}(\mathbf{L}_6+a^2\mathbf{L}_7), \tag{28}$$

$$\mathbf{L}_1=\begin{pmatrix} 0 & iN & \frac{\partial}{\partial\eta} & 0\\ -iq & 0 & -f'' & 0\\ 0 & -iq & 0 & 0\\ 0 & 0 & -iq & \frac{\partial}{\partial\eta}\end{pmatrix},$$

$$\mathbf{L}_2=\begin{pmatrix} 2 & 0 & 0 & 0\\ -2f' & 0 & 0 & 2\\ 0 & -2f' & 0 & 0\\ 0 & 0 & -2f' & 0\end{pmatrix}, \tag{29}$$

$$\mathbf{L}_3=\begin{pmatrix} 0 & 0 & 0 & 0\\ gNi & 0 & 0 & 0\\ 0 & gNi & g' & 0\\ 0 & 0 & gNi & 0\end{pmatrix},$$

$$\mathbf{L}_4=\begin{pmatrix} 1+\eta\frac{\partial}{\partial\eta} & 0 & 0 & 0\\ -\eta f'' & 0 & 0 & \eta\frac{\partial}{\partial\eta}\\ 0 & -f' & 0 & Ni\\ 0 & 0 & \eta f''+f' & 0\end{pmatrix}, \tag{30}$$

$$\mathbf{L}_5=\begin{pmatrix} 0 & 0 & 0 & 0\\ 0 & -2g & 0 & 0\\ \eta g' & 0 & 0 & 0\\ 0 & 0 & 0 & 0\end{pmatrix},\quad \mathbf{L}_6=\begin{pmatrix} 0 & 0 & 0 & 0\\ \frac{\partial^2}{\partial\eta^2} & 0 & 0 & 0\\ 0 & \frac{\partial^2}{\partial\eta^2} & 0 & 0\\ 0 & 0 & \frac{\partial^2}{\partial\eta^2} & 0\end{pmatrix}, \tag{31}$$

$$\mathbf{L}_7=\begin{pmatrix} 0 & 0 & 0 & 0\\ 1 & 0 & 0 & 0\\ 0 & 1 & 0 & 0\\ 0 & 0 & 1 & 0\end{pmatrix},\quad \mathbf{M}=\begin{pmatrix} 2 & 0 & 0 & 0\\ -2f' & 0 & 0 & 2\\ 0 & -2f' & 0 & 0\\ 0 & 0 & -2f' & 0\end{pmatrix}. \tag{32}$$

In the above expressions we have rescaled the azimuthal wave number and the nondimensional frequency,

$$N\equiv\frac{n}{R},\quad q\equiv\frac{\omega}{R}, \tag{33}$$

in order that some terms containing these parameters enter at the lowest order. The retained terms account for three different effects on the stability of the perturbations: (i) the effect of viscosity, (ii) the effect of the nonparallelism of the basic flow and of the amplitude of the perturbations, and (iii) the effect of the history, or convective evolution, of the perturbations. This last effect (iii) is described by the $\partial/\partial R$ terms of the stability equations, which are the ones responsible for the partial differential (though parabolic) character of the equations. All these three effects are therefore negligible in the limit $R\to\infty$ (or $\mathrm{Re}\to\infty$).

The above equations have to be solved with the following boundary conditions at $\eta=0$ and $\eta\to\infty$:

$$F(R,\infty)=G(R,\infty)=H(R,\infty)=0, \tag{34}$$

$$F(R,0)=G(R,0)=H(R,0)=0. \tag{35}$$

An initial condition at some large value of $R=R_i$ is also needed to solve Eq. (27). However, this last condition will not be used here because we shall look for local solutions (but retaining $\partial/\partial R$ terms) of the parabolized stability equations (see below).

As it stands there is some ambiguity in the partition of the perturbations (23) into two functions of the radial coordinate R. To close the problem one has to enforce an additional normalization condition which puts some restriction on the radial variation of the perturbation eigenfunction [11]. We shall perform here a local spatial stability analysis: Given a *real* frequency q and azimuthal wave number N, Eq. (27) and its R derivative will be solved locally for each radius $R=R_i$ with the *normalization* condition $[\partial a/\partial R]_{R=R_i}=0$. This condition will restrict, as required, the downstream variation of the perturbation eigenfunction, yielding, for each R, the local growth rate and radial wave number (or the phase speed of the disturbance) as functions of the axial distance to the plate η.

The eigenfunction $\mathbf{S}$ is expanded in a Taylor series about $R=R_i$, where only two terms are retained to be consistent with the approximations made in the previous section:

$$\mathbf{S}(R,\eta)\simeq\mathbf{S}(R_i,\zeta)+(R-R_i)\left.\frac{\partial\mathbf{S}(R,\eta)}{\partial R}\right|_{R=R_i} \equiv\mathbf{S}_0(\eta)+(R-R_i)\mathbf{S}_1(\eta). \tag{36}$$

This expansion is now substituted into Eq. (27) and its R derivative to obtain two equations for $\mathbf{S}_0$ and $\mathbf{S}_1$ ($|\mathbf{S}_1|\ll|\mathbf{S}_0|$).

Using the local normalization condition $[\partial a(R)/\partial R]_{R=R_i}=0$, one has

$$\mathbf{L}\cdot\mathbf{S}_0+\mathbf{M}\cdot\mathbf{S}_1=\mathbf{0}, \tag{37}$$

$$\mathbf{L}^*\cdot\mathbf{S}_0+\mathbf{M}^*\cdot\mathbf{S}_1=\mathbf{0}, \tag{38}$$

where the operator $\mathbf{L}$ is now evaluated at $R=R_i$ and

$$\mathbf{L}^*=\frac{\partial\mathbf{L}_1}{\partial R}-\frac{1}{2R^{2/3}}\mathbf{L}_3+\frac{1}{\sqrt{R}}\frac{\partial\mathbf{L}_3}{\partial R}+\frac{1}{2\sqrt{R}\,\mathrm{Re}^{3/(m+2)}}(\mathbf{L}_6+a^2\mathbf{L}_7), \tag{39}$$

$$\mathbf{M}^*=\mathbf{L}_1+a\mathbf{L}_2+\frac{1}{\sqrt{R}}\mathbf{L}_3+\frac{1}{R}\mathbf{L}_4-\frac{\sqrt{R}}{\mathrm{Re}^{3/(m+2)}}(\mathbf{L}_6+a^2\mathbf{L}_7). \tag{40}$$

For given q, n, and $R=R_i$, this constitutes a nonlinear eigenvalue problem for the complex eigenvalue a and the complex eigenfunction

$$\mathbf{X}(\eta)\equiv\begin{pmatrix}\mathbf{S}_0\\ \mathbf{S}_1\end{pmatrix}. \tag{41}$$

One is interested in looking for convective instabilities propagating towards the axis—i.e., in the same direction as the radial basic flow. Thus, for a given positive value of q, one is interested in modes whose eigenvalue a has both its real and imaginary parts negative. According to Eqs. (25) and (26), this ensures that the perturbation grows exponentially as it propagates towards decreasing R ($\gamma<0$), with phase velocity directed towards the axis (i.e., $\alpha<0$). We are mostly interested in the evolution as R decreases the most unstable mode (largest $|\gamma|$) for given values of q and n and in how this evolution depends on the distance η to the plate. To that end we define a nondimensional *physical* growth rate γ_u and a nondimensional *physical* radial wave number α_u based on the radial velocity component of the perturbation $(u_0\bar{u})$:

$$a_u\equiv-\frac{\delta}{\bar{u}u_0}\frac{\partial}{\partial r}(\bar{u}u_0)=-\frac{1}{F\chi}\left(\frac{\partial F}{\partial R}\chi+aF\chi\right)=-a-\frac{1}{F}\frac{\partial F}{\partial R}, \tag{42}$$

$$\gamma_u(R,\eta)=\mathrm{Re}(a_u)=-\gamma(R)-\mathrm{Re}\left[\frac{F_1(\eta)}{F_0(\eta)}\right], \tag{43}$$

$$\alpha_u(R,\eta)=\mathrm{Im}(a_u)=-\alpha(R)-\mathrm{Im}\left[\frac{F_1(\eta)}{F_0(\eta)}\right], \tag{44}$$

where $F_0(\eta)=F(R_i,\eta)$ and $F_1(\eta)=[\partial F(R,\eta)/\partial R]_{R=R_i}$ (for simplicity, in the above expressions and in what follows, we write R for R_i). The nondimensional local phase speed of the disturbances is defined in terms of α_u:

$$c_u(R,\eta)\equiv\frac{q}{\alpha_u(R,\eta)}. \tag{45}$$

Finally, to measure the global growth rate of the disturbances, it is convenient to define an integral growth rate

$$\gamma_u^I(R)=\frac{\int_0^\infty\gamma_u(R,\eta)|F(R,\eta)|d\eta}{\int_0^\infty|F(R,\eta)|d\eta}, \tag{46}$$

which is more appropriate than the real part of the eigenvalue $-\gamma$ to characterize the amplification rate of the perturbations. Note that $\gamma_u^I\to-\gamma$ for $R\to\infty$.

Alternatively, one may use a nondimensional physical growth rate γ_v based on the azimuthal velocity component of the perturbation $(u_0\bar{v})$:

$$\gamma_v(R,\eta)=-\gamma(R)-\mathrm{Re}\left[\frac{G_1(\eta)}{G_0(\eta)}\right], \tag{47}$$

where $G_0(\eta)=G(R_i,\eta)$ and $G_1(\eta)=[\partial G(R,\eta)/\partial R]_{R=R_i}$ and the corresponding integral growth rate

$$\gamma_v^I(R)=\frac{\int_0^\infty\gamma_v(R,\eta)|G(R,\eta)|d\eta}{\int_0^\infty|G(R,\eta)|d\eta}. \tag{48}$$

Since all the velocity components of the perturbations are of the same order of magnitude, we shall use γ_v^I or γ_u^I depending on the numerical precision of the corresponding eigenfunction component.

To solve Eqs. (37) and (38) numerically, the η dependence of $\mathbf{X}$ is discretized using a staggered Chebyshev spectral collocation technique developed by Khorrami [12]. This method has the advantage of eliminating the need of two artificial pressure boundary conditions at $\eta=0$ and $\eta=\infty$, which for that reason are not included in Eqs. (34) and (35). The boundary conditions at infinity are applied at a truncated radial distance η_{max}, chosen large enough to ensure that the results do not depend on that truncated distance (values of η_{max} between 250 and 600 were used in the computations reported below). To implement the spectral numerical method, Eqs. (37) and (38) are discretized by expanding $\mathbf{X}$ in terms of truncated Chebyshev series. A nonuniform coordinate transformation is used to map the interval $0\leqslant\eta\leqslant\eta_{max}$ into the Chebyshev polynomial domain $-1\leqslant s\leqslant 1$:

$$\eta=c_1\frac{1-s}{c_2-s},\quad\text{with } c_2=1+\frac{2c_1}{\eta_m}, \tag{49}$$

and c_1 is a constant such that approximately half of the nodes are concentrated in the interval $0\leqslant\eta\leqslant c_1$. This transformation allows large values of η to be taken into account with relatively few basis functions.

The η domain is thus discretized in N_z points, N_z being the number of Chebyshev polynomials in which $\mathbf{X}$ has been expanded. In the results presented here, N_z ranged between 140 and 200. With this discretization, Eqs. (37) and (38) become an algebraic nonlinear eigenvalue problem which is solved using the linear companion matrix method described by Bridges and Morris [13]. The resulting (complex) linear eigenvalue problem is solved with double precision using an eigenvalue solver. In particular, we have used one solver

from the IMSL library, which provides the entire eigenvalue and eigenvector spectrum. Since the dimension of the associated linear problem is $16N_z$, the computation time increases very fast with the number of nodal points N_z. Also, due to the large dimension of the matrices, a relatively large amount of spurious numerical eigenvalues are produced by the eigenvalue solver, particularly when q is very small. They are, however, easily discarded because the corresponding growth rates change wildly as N_z increases, instead of rapidly converging to a finite value, as happens for eigenvalues of the physical modes.

IV. RESULTS

A. Inviscid and parallel results

We shall consider first the inviscid or inertial instabilities for $R\to\infty$, $\sqrt{R}/\mathrm{Re}^{3/(m+2)}\to 0$. In this limit, the above stability equations can be written as ($m=1$ and $L=\sqrt{2}$ in what follows)

$$H' + iGN + 2aF = 0, \tag{50}$$

$$-iqF - 2f'aF - f''H + 2a\Pi = 0, \tag{51}$$

$$-iqG - 2f'aG + \frac{1}{\sqrt{R}}(Hg' + gGiN) = 0, \tag{52}$$

$$-iqH - 2f'aH + \Pi' = 0, \tag{53}$$

where the primes denote differentiation with respect to η. Eliminating F, G, and Π, one is left with a single Rayleigh-type equation for H,

$$H'' + \left(4a^2 - \frac{2af'''}{iq + 2af'}\right)H = 0, \tag{54}$$

with the boundary conditions

$$H(0) = 0, \quad H(\infty) = 0. \tag{55}$$

The remaining eigenfunctions are related to H through

$$G = \frac{Hg'}{\sqrt{R}(iq + 2f'a)}, \tag{56}$$

$$F = \frac{1}{2a}H', \quad \Pi' = (iq + 2f'a)H. \tag{57}$$

We have retained some terms proportional to $R^{-1/2}$ in order to account for almost inviscid perturbations with some swirl component ($G\neq 0$). But in the formal inviscid limit $R\to\infty$, all the relevant perturbations have no swirl component [$G=0$; see Eq. (56)] and are *axisymmetric* ($N\to 0$ for $R\to\infty$ and n finite).

For real frequency q, Eqs. (54) and (55) constitute a cubic eigenvalue problem for the complex eigenvalue a and the complex eigenfunction H. For $q=0$, the problem has no solution, except for the trivial one $a=0$. For each $q>0$, if H is an eigenfuction with eigenvalue a, then so too is $-H^\dagger$ with eigenvalue $-a^\dagger$, where $\dagger$ denotes the complex conjugate, for the same q. Thus, to each mode with growth rate γ and wave number α there is a corresponding mode with growth rate $-\gamma$ and the same α—i.e., the same phase velocity. If $\alpha<0$, the wave propagates towards the axis (decreasing R), so that the mode with $\gamma<0$ is unstable, while the corresponding mode with $\gamma>0$ is stable. Conversely, for $\alpha>0$, the mode with $\gamma>0$ is unstable and its counterpart with $\gamma<0$ is stable. As discussed in the previous section, we shall look for unstable modes propagating towards the axis ($\alpha<0$ and $\gamma<0$).

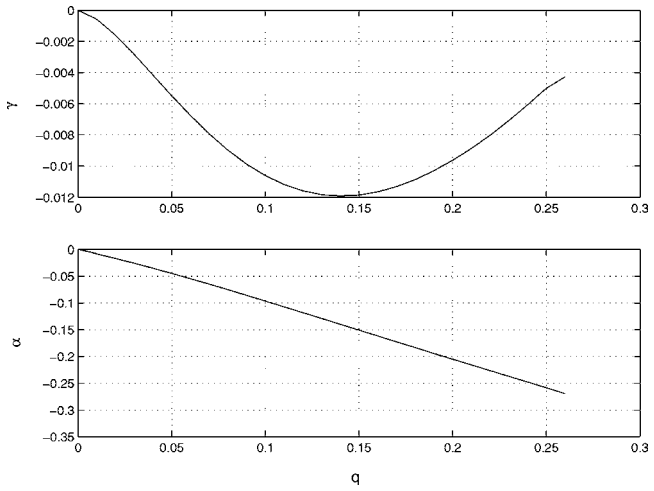

FIG. 4. Growth rate (γ) and axial wave number (α) vs frequency (q) for the most unstable inviscid modes ($R\to\infty$).

The cubic eigenvalue problem (54) and (55) is numerically solved using the linear companion matrix method [13]. First, Eq. (54) is discretized in N_z nodes by a spectral collocation method, so that the associated linear eigenvalue problem has dimension $3N_z$ (we use $N_z=350$ in the computations). Figure 4 shows the real and imaginary parts of a as functions of q corresponding to the most unstable modes (highest values of $|\gamma|$) propagating towards the axis—i.e., with negative values of both γ and α. Since $\alpha(q)$ is almost a straight line, the group velocity of the perturbations, $c_g = \partial q/\partial\alpha$, practically coincides with the phase speed $c_f = q/\alpha$, which therefore is also negative, as it should for wave packets traveling towards the axis. Note also that the relevant values of q are small as a consequence of the scaling (33).

The eigenfunctions corresponding to the most unstable inviscid perturbations ($q=q^*\simeq 0.14$) are plotted in Fig. 5. It should be noted that in the present inviscid limit, the integral growth rate $\gamma^I_{u,v} = |\gamma|$.

B. Nonparallel and viscous results for $n=0$

We now consider viscous and nonparallel effects (R and Re finite, but large) for axisymmetric perturbations. For each value of R and $n=0$, we select the less stable mode as a function of the frequency q. For very large values of R the results obviously coincide with the inviscid results of the previous section. These inertial unstable modes first tend to be more unstable as R decreases, and then their maximum growth rate decreases. In addition, a different unstable *viscous* mode emerges for finite R that eventually becomes the most unstable one as R decreases. All these features may be observed in Figs. 6–11.

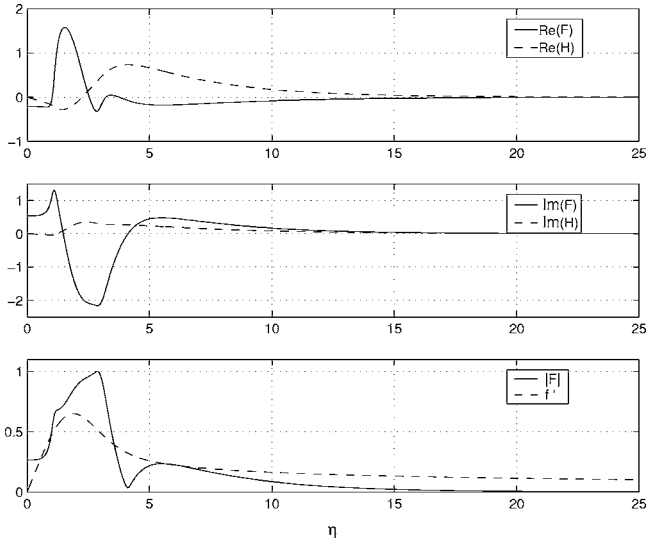

FIG. 5. Eigenfunctions for the most unstable inviscid mode corresponding to $q=q^{*}\simeq 0.14$. Also plotted for reference sake is f'.

Figure 6 shows the integral growth rate γ^I as a function of q of both the most unstable inertial and viscous modes for several values of R. It must be noted that we have used γ_u^I for large R and γ_v^I for moderate R (see also Fig. 10 below). The reason for this choice is that, for large R, the azimuthal component G of the eigenfunction is very small (as discussed in the previous section, the inertial mode has no swirl, $G=0$, for $R\to\infty$), so that G is not appropriate to compute the physical growth rate (γ_v), and we use F to compute γ_u. As R decreases, G becomes of the same order of magnitude as F (see Figs. 7 and 8). At the same time, F becomes more extended in space and one needs more and more points to have F_0 and F_1 with precision enough to compute γ_u. For $R<10^3$, approximately, the number of points needed to have γ_u with precision enough is already so large that the computation time and memory become prohibitive. However, G_0 and G_1 remain sufficiently concentrated near the plane $\eta=0$, even for relatively small values of R (G practically vanishes for $\eta>5$; see Figs. 7 and 8), that γ_v can be computed with very high precision using a relatively small number of nodes. This is corroborated in Fig. 9, where γ_v^I is plotted as a function of the value η_{int} at which the integrals in Eq. (48) are truncated, using different N_z and η_{max}, for a relatively small value of R. It is seen that the resulting γ_v^I remains practically unchanged for $\eta>5$ (in contrast, to compute γ_u^I for this R one would need a much higher value of η_{int}, and the number of nodes N_z to obtain it with precision enough would be numerically prohibitive).

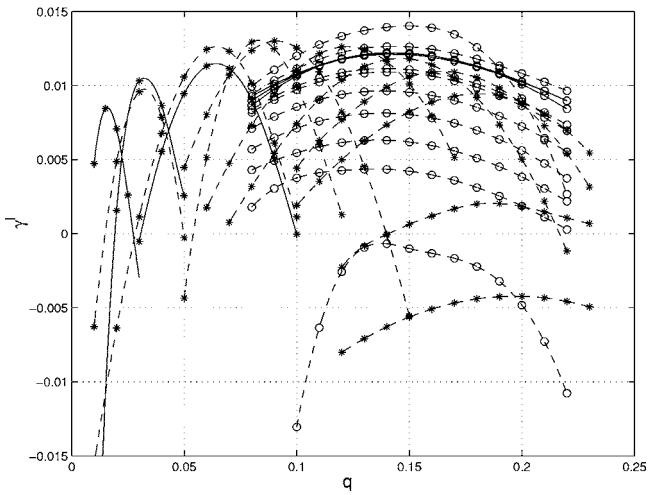

FIG. 6. Integral growth rate vs nondimensional frequency for the less stable inertial modes (○) and viscous modes (∗) for several values of R. Solid lines correspond to γ_u^I, while dashed lines correspond to γ_v^I. The different values of R plotted correspond to the symbols in Fig. 10.

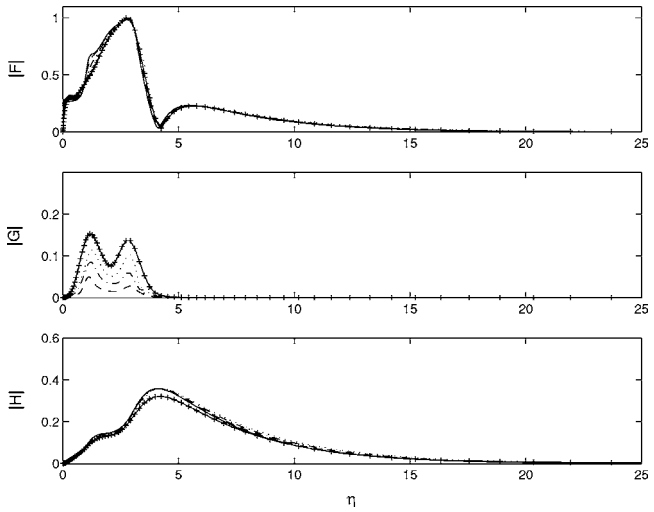

FIG. 7. Eigenfunctions for the most unstable *inertial* modes for different values of R: $R\to\infty$ (solid line), $R=2714.4$ (dashed line), $R=584.8$ (dot-dashed line), $R=262.1$ (dotted line), and $R=126.0$ (+). The maximum value of $|F|$ is normalized to unity in all the cases.

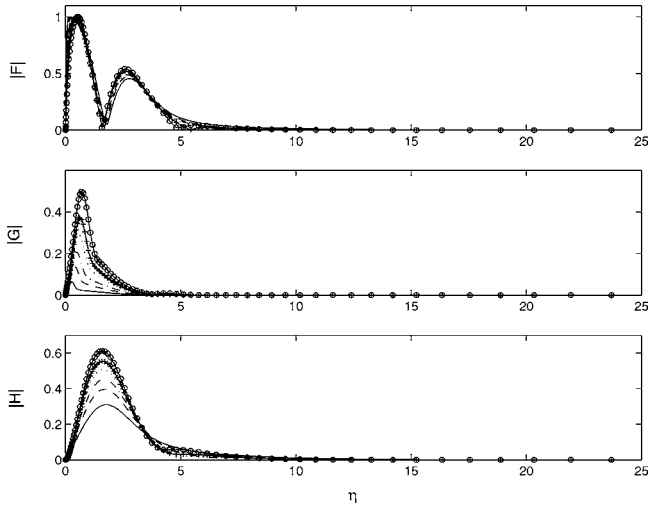

FIG. 8. Eigenfunctions for the most unstable *viscous* modes for different values of R: $R=2714.4$ (solid line), $R=584.8$ (dashed line), $R=262.1$ (dot-dashed line), $R=126.0$ (dotted line), $R=79.4$ (+), and $R=43.1$ (○). The maximum value of $|F|$ is normalized to unity in all the cases.

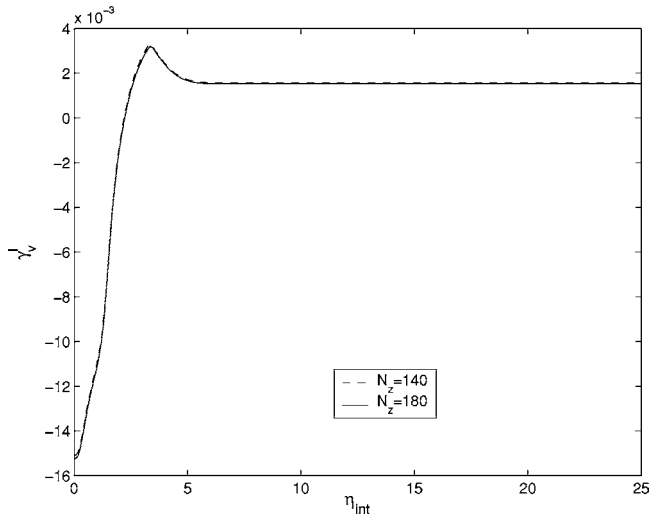

FIG. 9. γ_v^I as a function of the η_{int} at which the integrals in Eq. (48) are truncated for two values of N_z, as indicated. $R=27$, $n=0$, $q=0.22$; $\eta_{max}=500$ ($N_z=140$), $\eta_{max}=600$ ($N_z=180$).

The maximum values of $\gamma_{u,v}^I$ (denoted by γ_{max}^I) and their corresponding frequencies and axial wave numbers q_{max} and α_{max} are plotted in Figs. 10 and 11 as functions of R, both for viscous and inviscid modes. It is observed that γ_{max}^I for the inviscid mode undergoes a discontinuity at $R \simeq 500$. In addition, below this Reynolds number, the inertial mode is no longer the most unstable one, becoming the viscous mode more unstable. As R decreases further, the growth rate of both modes decreases, until they become stable for $R \simeq 28.6$ (inviscid modes) and $R \simeq 25.6$ (viscous modes; see Fig. 10).

C. Nonparallel and viscous results for $n \neq 0$

Since the azimuthal wave number n enters the stability equations as $N=n/R$, the stability properties of the nonaxisymmetric perturbations differ very little from the axisymmetric ones when R is large. For this reason, we have considered only the viscous modes for these spiral perturbations ($n \neq 0$) and for values of R near their critical ones, where the differences with the axisymmetric results become appreciable. Actually, we only report here the critical values R_n^c below which these viscous, nonaxisymmetric modes become stable (Table I and Fig. 12). It is observed that, for counterrotating perturbations ($n<0$), the critical values of R are larger than $R_{n=0}^c$. For corotating perturbations ($n>0$), the critical Reynolds numbers are smaller than for axisymmetric perturbations, until a minimum is reached for $n=4$ ($R_4^c = R_{min}^c \simeq 23$), and then the critical value of R increases as $n \to \infty$. Thus, the last perturbations that become stabilized by viscosity as the axis is approached are spiral perturbations with $n=4$.

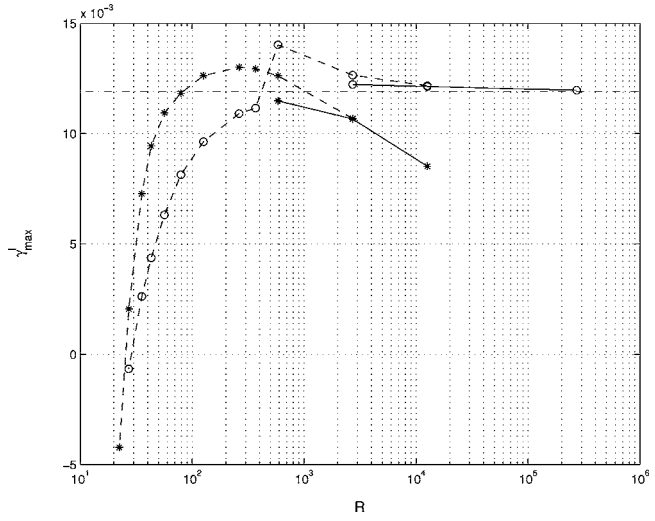

FIG. 10. Maximum values of the integral growth rate vs R for the inertial modes (○), and for the viscous modes (∗). Solid lines correspond to γ_u^I, while dashed lines correspond to γ_v^I. The dash-dotted horizontal line corresponds to the inviscid limit $R \to \infty$.

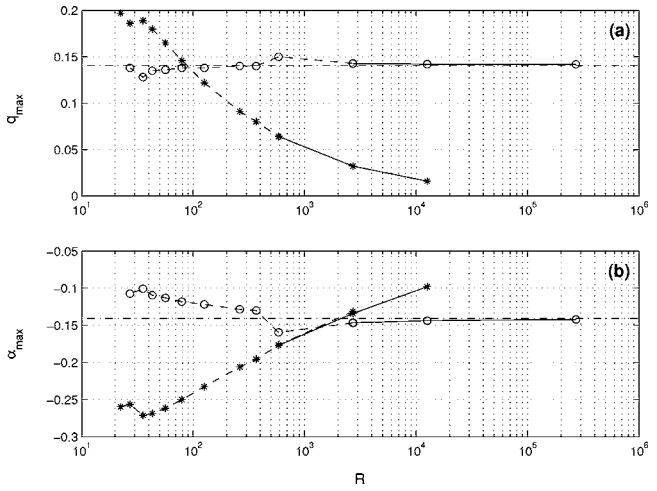

FIG. 11. Frequencies (a) and axial wave numbers (b) corresponding to the maximum values of the integral growth rate vs R plotted in Fig. 10.

V. CONCLUSIONS

In this work we have analyzed the spatial stability of the viscous boundary layer induced by a free vortex, which near the axis coincides with Long's vortex, on a solid plane perpendicular to its axis. Viscous and nonparallel effects have been taken into account consistently in the evolution of the perturbations towards the axis.

For large Reynolds numbers (i.e., far away from the axis, $R \to \infty$), the flow is inertially unstable for axisymmetric per-

TABLE I. R^c for several values of n.

n	Re^c	n	Re^c
−2	27.8115	4	22.9849
−1	26.4338	5	23.1792
0	25.6430	6	23.6662
1	24.7337	7	24.3608
2	23.7901	8	25.0700
3	23.1772	10	26.3457

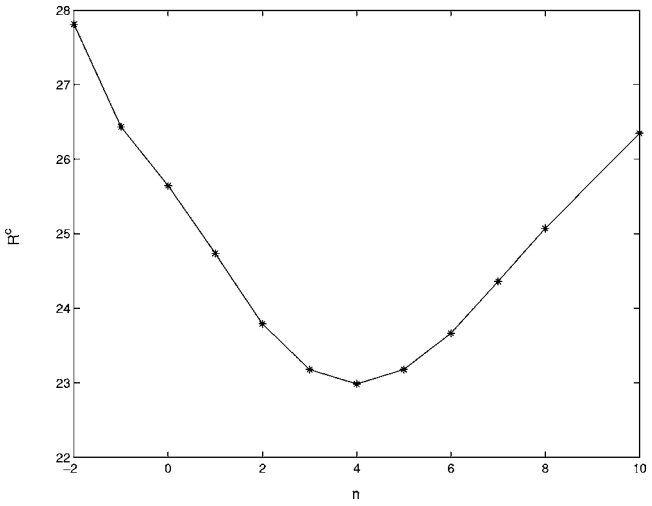

FIG. 12. Critical values of R for the most unstable viscous modes as functions of the azimuthal wave number n.

turbations ($n=0$). As the axis is approached (R decreases), new *viscous* instabilities are found that become more unstable than the *inertial* ones for $R<R^+\simeq 500$. These viscous instabilities appear for both axisymmetric and nonaxisymmetric perturbations, and eventually all of them become stabilized by viscosity as the axis is approached. We find that the last perturbations that become stable as R decreases are nonaxisymmetric, corotating perturbations with azimuthal wave number $n=4$, though all the critical Reynolds numbers for the different values of n are in fact very close (see Fig. 12). The minimum critical Reynolds number at which the perturbations with $n=4$ become stable is found to be $R^c_{min}\simeq 23$, which corresponds to a vortex Reynolds number $\mathrm{Re}\simeq 1103$. Since this critical value is sufficiently large for the boundary layer approximation to remain valid, these results show that one may use the present viscous boundary layer vortex as axisymmetric boundary conditions for the (3D) numerical simulation of the Navier-Stokes equations to find out the structure of the effusing core flow turning upwards near the axis, provided that the inlet flow is taken at moderate, but high, Reynolds numbers.

ACKNOWLEDGMENT

This work has been supported by the Ministerio de Educación y Ciencia of Spain (Grant No. FIS04-00538).

[1] R. R. Long, J. Fluid Mech. **11**, 611 (1961).
[2] O. R. Burggraf and M. R. Foster, J. Fluid Mech. **80**, 685 (1977).
[3] V. Shtern and F. Hussain, Phys. Fluids A **5**, 2183 (1993).
[4] R. Fernandez-Feria, J. Fernandez de la Mora, and A. Barrero, J. Fluid Mech. **305**, 77 (1995).
[5] R. Fernandez-Feria and J. C. Arrese, Q. J. Mech. Appl. Math. **53**, 609 (2000).
[6] W. R. C. Phillips, Phys. Fluids **27**, 2215 (1984).
[7] A. Ogawa, *Vortex Flows* (CRC Press, London, 1993).
[8] R. Fernandez-Feria, J. Fernandez de la Mora, M. Perez-Saborid, and A. Barrero, Q. J. Mech. Appl. Math. **52**, 1 (1999).
[9] W. S. King and W. S. Lewellen, Phys. Fluids **7**, 1674 (1964).
[10] O. R. Burggraf, K. Stewartson, and R. J. Belcher, Phys. Fluids **14**, 1821 (1971).
[11] F. P. Bertolotti, Th. Herbert, and P. R. Spalart, J. Fluid Mech. **242**, 441 (1992).
[12] M. R. Khorrami, Int. J. Numer. Methods Fluids **12**, 825 (1991).
[13] T. J. Bridges and P. J. Morris, J. Comput. Phys. **55**, 437 (1984).